Numerical Investigations to quantify the effect of Horizontal Membranes on the performance of a Fluidized Bed Reactor

Robert Hommel[1], Schalk Cloete[1] and Shahriar Amini[1]*

1) Flow Technology group, Department of Process Technology, SINTEF Materials and Chemistry, Trondheim, Norway

*Corresponding author. Email: shahriar.amini@sintef.no
Address: SINTEF Materials and Chemistry, Richard Birkelands Vei 3, 7034 Trondheim, Norway, Phone: +47 46639721

1 Abstract

Reactive simulations of gas-solid flows occurring in fluidized beds with horizontal membrane insertion were carried out using computational fluid dynamics based on the kinetic theory of granular flows. The effect of altering the membrane arrangement on the overall reactor performance (degree of conversion achieved) was investigated by means of fractional factorial designs. When membranes served only as hydrodynamic modifiers to the flow, it was found that significant improvements could be obtained by optimising the membrane arrangement. A slightly larger improvement could be attained by injecting some of the reacting gas through the membranes. When compared to the improvements that can be attained by simply scaling up the reactor height and especially the reactor width, however, these improvements were of less significance. The use of membranes solely for altering reactor hydrodynamics by serving as obstructions and gas injection points can therefore not be merited. Further optimisation studies into membrane arrangement are therefore only recommended for specific processes in which the membranes play a central role by extracting some of the process gasses.

Keywords: Fluidized bed; Reactor; Granular flow; Membrane; Computational fluid dynamics, Kinetic theory of granular flows

2 Introduction

Membrane assisted fluidized bed reactors have recently enjoyed a substantial amount of research attention. A large number of potential advantages linked to such applications have been identified in a recent review paper [1]. Primarily, the

selective dosing/removal of reactants/products grants much greater process control and can be used to circumvent thermodynamic equilibrium restrictions. This characteristic can lead to significant improvements in existing process performance and offers a number of interesting potentials for future process development.

The combination of membrane and fluidized bed technology seems to be favourable since the inclusion of membranes has been shown to alter reactor hydrodynamics such that gas-emulsion mass transfer is improved. Membrane insertion does, however, increase the complexity of the already complex fluidized bed reactor by adding extra degrees of freedom to the design process. The number, size, positioning, orientation and type of membranes are additional variables that have to be specified.

Numerical modelling offers an ideal framework for initial investigations into the possible advantageous effects that could result from the manipulation of such membrane variables. A large number of reactor setups can be evaluated in a timely and economic manner without any of the practical restrictions that would be imposed by physical experimentation. Quantification of reactor improvement is also much clearer due to the complete and easily accessible flow data offered by these simulations.

The kinetic theory of granular flows (KTGF) [2-4] is a generally accepted method for simulating gas-solid flows in bubbling fluidized beds. This approach has been validated in standard bubbling beds [5] and has been used in numerous fluidized bed simulation studies since. The application of the KTGF to membrane assisted fluidized bed reactors has not been as thoroughly explored though. One study [6] has shown that the Eulerian-Eulerian two fluid model (TFM) with closure relations derived from the KTGF successfully predicted the bubble characteristics, bubble breakup behaviour and rise velocity in a bed with inserted tubes. These are the most important membrane induced effects to be captured and the KTGF can therefore be assumed to sufficiently capture the system behaviour when membranes are inserted into the domain.

A reactive membrane assisted fluidized bed reactor (MAFBR) will be simulated in this study. Reactive fluidized bed systems have been simulated using KTGF-approaches [7-9], but thorough validation is still lacking. This study will only compare different design scenarios, however, and therefore does not require thorough quantitative reaction kinetic validation. Qualitative trends between simulations should be well captured by the reactive flow model if the hydrodynamics are accurately predicted.

The fact that horizontally immersed tubes in fluidized beds have a significant influence on the hydrodynamics is already shown and well known [6, 10, 11]. Deshmukh et al. [10] studied experimentally the extent of gas back mixing for MAFBRs. It was found that the presence of membranes reduced the extent of

gas back-mixing. Further investigations revealed that an addition of gas via the horizontal membranes reduced the gas back mixing even further.

The aforementioned simulation study [6] of a bubbling fluidized bed containing staggered horizontal tubes compared with experimental results [11] to confirm that the presence of horizontal tubes obstruct the lateral movement of the bubbles, which results in a reduction of the bubble diameter and a decrease in bubble rise velocity in the vicinity of the tubes. The smaller bubble diameter results in an enlarged surface area between the gas and the solids phase and the lower rise velocity causes a longer interaction time. Both these effects are expected to be beneficial in terms of reactor performance by increasing the reaction rate.

This potential improvement in reactor performance has not been quantified as of yet. The present study will therefore be undertaken to assess whether the potential for improvement due to the aforementioned membrane effects is large enough to merit significant further research effort. A hypothetical catalytic reaction will be implemented in order to get a direct measure of how ultimate reactor performance is impacted by the presence of membranes. Possible improvements in reactant conversion caused by the presence of membranes can then be compared against the improvements to be gained from a process scale-up in order to judge the potential.

3 Simulation

3.1 Model equations

The numerical simulation was carried out using the Eulerian multifluid model. In this framework, the conservation equations are solved for each phase present in the simulation. Two phases, gas and solids, were included in the present study.

3.1.1 Conservation equations

The continuity equations for the gas and solids phases are given below:

$$\frac{\partial}{\partial t}\left(\alpha_g \rho_g\right) + \nabla \cdot \left(\alpha_g \rho_g \vec{v}_g\right) = 0 \tag{1}$$

$$\frac{\partial}{\partial t}\left(\alpha_s \rho_s\right) + \nabla \cdot \left(\alpha_s \rho_s \vec{v}_s\right) = 0 \tag{2}$$

The conservation of momentum for the gas phase is written as follows:

$$\frac{\partial}{\partial t}\left(\alpha_g \rho_g \vec{\upsilon}_g\right) + \nabla \cdot \left(\alpha_g \rho_g \vec{\upsilon}_g \vec{\upsilon}_g\right) = -\alpha_g \nabla p + \nabla \cdot \bar{\bar{\tau}}_g + \alpha_g \rho_g \vec{g} + K_{sg}\left(\vec{\upsilon}_s - \vec{\upsilon}_g\right) \tag{3}$$

And for the solids as:

$$\frac{\partial}{\partial t}\left(\alpha_s \rho_s \vec{\upsilon}_s\right) + \nabla \cdot \left(\alpha_s \rho_s \vec{\upsilon}_s \vec{\upsilon}_s\right) = -\alpha_s \nabla p - \nabla p_s + \nabla \cdot \bar{\bar{\tau}}_s + \alpha_s \rho_s \vec{g} + K_{gs}\left(\vec{\upsilon}_g - \vec{\upsilon}_s\right) \tag{4}$$

Species are also conserved for the gas phase.

$$\frac{\partial}{\partial t}\left(\alpha_g \rho_g Y_{g,i}\right) + \nabla \cdot \left(\alpha_g \rho_g \vec{\upsilon}_g Y_{g,i}\right) = \nabla \cdot \alpha_g \vec{J}_{g,i} + \alpha_g S_{g,i} \tag{5}$$

No energy conservation was included under the assumption of isothermal flow. This is usually a good assumption due to the excellent mixing achieved in fluidized bed reactors.

3.1.2 Closures

The KTGF was implemented to model solids stresses resulting from particle collisions and uncorrelated translations. Kinetic energy contained in the random particle motions is quantified in terms of granular temperature and can be written in conservation form as follows:

$$\frac{3}{2}\left[\frac{\partial}{\partial t}\left(\alpha_s \rho_s \Theta_s\right) + \nabla \cdot \left(\alpha_s \rho_s \vec{\upsilon}_s \Theta_s\right)\right] = \left(-p_s \bar{\bar{I}} + \bar{\bar{\tau}}_s\right) : \nabla \vec{\upsilon}_s + \nabla \cdot \left(k_{\Theta_s} \nabla \Theta_s\right) - \gamma_{\Theta_s} + \phi_{gs} \tag{6}$$

In the present study, this equation was solved in its algebraic form by neglecting the contributions of convection and diffusion. This is a good assumption in dense and slow moving bubbling beds since the local generation and dissipation strongly outweighs contributions from convective and diffusive fluxes. Equation (6) is therefore solved algebraically based on the local balance of granular temperature generation due to solids stresses and dissipation due to inelastic collisions and damping by the primary phase. Collisional dissipation of energy is expressed as [12]

$$\gamma_{\Theta_s} = \frac{12\left(1 - e_{ss}^2\right) g_{0,ss}}{d_s \sqrt{\pi}} \rho_s \alpha_s^2 \Theta_s^{3/2} \tag{7}$$

and the interphase fluctuating energy transfer (damping by primary phase) as [4]

$$\phi_{gs} = -3K_{gs}\Theta_s \tag{8}$$

The granular temperature is subsequently used to calculate values of the solids viscosity for implementation in the solids stress tensor. Bulk and shear viscosities occur due to particle translation and collision in the solids phase. The bulk viscosity is calculated as follows [12]:

$$\lambda_s = \frac{4}{3}\alpha_s \rho_s d_s g_{0,ss}\left(1+e_{ss}\right)\left(\frac{\Theta_s}{\pi}\right)^{1/2} \tag{9}$$

Shear viscosity consists of three parts: collisional, kinetic and frictional. The collisional part is calculated as [3, 4]

$$\mu_{s,col} = \frac{4}{5}\alpha_s \rho_s d_s g_{0,ss}\left(1+e_{ss}\right)\left(\frac{\Theta_s}{\pi}\right)^{1/2} \tag{10}$$

the kinetic part as [4]

$$\mu_{s,kin} = \frac{10\rho_s d_s\sqrt{\Theta_s \pi}}{96\left(1+e_{ss}\right)g_{0,ss}}\left[1+\frac{4}{5}\alpha_s g_{0,ss}\left(1+e_{ss}\right)\right]^2 \tag{11}$$

and the frictional part as [13]

$$\mu_{s,fr} = \frac{p_s \sin\varphi}{2\sqrt{I_{2D}}} \tag{12}$$

Modelled bulk and shear viscosities are used in the solids stress tensor in equation (4) as follows:

$$\overline{\overline{\tau}}_s = \alpha_s \mu_s\left(\nabla\vec{\upsilon}_s + \nabla\vec{\upsilon}_s^T\right) + \alpha_s\left(\lambda_s - \frac{2}{3}\mu_s\right)\nabla\cdot\vec{\upsilon}_s\overline{\overline{I}} \tag{13}$$

The solids pressure used in equation (12) as well as in equation (4) is calculated according to Lun *et al.* [12]:

$$p_s = \alpha_s \rho_s \Theta_s + 2\rho_s \left(1 - e_{ss}\right) \alpha_s^2 g_{0,ss} \Theta_s \tag{14}$$

The radial distribution function which is a measure of the average distance between particles is a central concept in the KTGF and is calculated as [14]

$$g_{0,ss} = \left[1 - \left(\frac{\alpha_s}{\alpha_{s,\max}} \right)^{1/3} \right]^{-1} \tag{15}$$

Inter-phase momentum exchange was modelled according to Syamlal et al. [3].

$$C_D = \left(0.63 + \frac{4.8}{\sqrt{\mathrm{Re}_s / \upsilon_{r,s}}} \right)^2 \tag{16}$$

$$\upsilon_{r,s} = 0.5\left(A - 0.06\,\mathrm{Re}_s + \sqrt{\left(0.06\,\mathrm{Re}_s\right)^2 + 0.12\,\mathrm{Re}_s\left(2B - A\right) + A^2} \right) \tag{17}$$

$$A = \alpha_g^{4.14} \tag{18}$$

$$\begin{aligned} B &= 0.8\alpha_g^{1.28} && \alpha_g \le 0.85 \\ B &= \alpha_g^{2.65} && \alpha_g > 0.85 \end{aligned} \tag{19}$$

$$\mathrm{Re}_s = \frac{\rho_g d_s \left| \vec{\upsilon}_s - \vec{\upsilon}_g \right|}{\mu_g} \tag{20}$$

The drag coefficient and the resulting drag force determines the inter-phase momentum exchange coefficient in equations (3) and (4).

$$f = \frac{C_D\,\mathrm{Re}_s\,\alpha_g}{24\upsilon_{r,s}^2} \tag{21}$$

$$K_{gs} = K_{sg} = \frac{\alpha_s \rho_s f}{\tau_s} \tag{22}$$

$$\tau_s = \frac{\rho_s d_s^2}{18\mu_g} \tag{23}$$

Reaction kinetics were implemented using the shrinking core model [15] with reaction rate as the limiting step. A simple, catalytic conversion of gas species A to gas species B was simulated to occur on the surface of microscopic solid grains (*S*) within the particles used in the fluidized bed: $A + S \rightarrow B + S$

The physical properties of species A and B were specified to be identical so that the reaction would not influence the hydrodynamics resulting in a non-linear interaction. This will significantly simplify the interpretation of results.

When reaction rate control is assumed with the shrinking core model, the rate of consumption of species A on the surface of the unreacted core can be expressed as follows:

$$-\frac{dN_A}{dt} = \pi d_c^2 k C_A^n \tag{24}$$

This relation can be rewritten in terms of a volumetric heterogeneous reaction rate that can be implemented into the CFD code:

$$R^H = -\frac{1}{V}\frac{dN_A}{dt} = \frac{6}{d_{gr}}\alpha_s k\left(\frac{\alpha_g x_A \rho_g}{M_A}\right) \tag{25}$$

Equation (25) is formulated on the assumption that the reaction takes place at an equal rate on all the grains inside the particle. It is also assumed that there is no shrinkage of the unreacted core since a catalytic reaction was simulated. The reaction was considered to be first order. It can be seen from equation (25) that the local reaction rate is proportional to both the solids concentration and the mass fraction of species A. Better gas-solid contact (higher solids concentration) and reduced gas back-mixing (higher reacting species concentration) will therefore increase the simulated reaction rate.

The hypothetical reaction rate constant given in equation (26) was implemented. Both the pre-exponential factor and the activation energy are representative of real materials used in reacting fluidized bed systems such as Ilmenite and various other metal oxides. The reaction was assumed to occur at a temperature of 900°C.

$$k = 0.1e^{(-100000/RT)} \tag{26}$$

The calculated reaction rate is used to determine the species transfer rate for implementation as a source term in equation (5).

$$S_{g,B} = -S_{g,A} = R^H M_A \tag{27}$$

Since the stoichiometric ratio of the simulated reaction is 1:1 and the properties of species A and B were specified to be identical, no mass or momentum source terms are required.

3.2 Boundary Conditions

A simple no-slip wall boundary condition was set for the gas phase. The partial slip Johnson and Jackson [16] boundary condition was used for the granular phase with a specularity coefficient of 0.5.

$$\vec{\tau}_s = -\frac{\pi}{6}\sqrt{3}\varsigma\frac{\alpha_s}{\alpha_{s,\max}}\rho_s g_{0,ss}\sqrt{\Theta_s}\vec{U}_{s,\|} \tag{28}$$

This value was found to give the best comparison to the experimental data of Taghipour *et al.* [5] on which the current simulated geometry is based. A fixed velocity of 0.5 m/s was specified at the inlet. The incoming gas consisted only of species A. The outlet was specified as a pressure outlet at atmospheric pressure.

3.3 Flow solver and solver settings

The commercial software package, FLUENT 12.1.2 was used as the solver. The phase coupled SIMPLE scheme [17] was used for pressure-velocity coupling and the higher order QUICK scheme [18] for the spatial discretization of all remaining equations. First order implicit temporal discretization was used.

3.4 Geometry

A 2D plane geometry, 0.28 m in width and 1 m in high, was used to simulate the fluidized bed. The bed dimensions were based on a validated simulation [5] in order to increase confidence in model results. The geometry was divided into two zones: the bed zone with a height of 0.8 m and a porous zone for the remaining 0.2 m at the top. The porous zone was specified in order to achieve plug flow and prevent backflow at the outlet. Graphical representations of the geometry with different membrane configurations can be viewed in Table 3 and Table 6.

3.5 Simulation summary

A summary of physical properties and simulation parameters is given in Table 1.

Table 1: Physical properties and simulation parameters

Gas density (species A and B)	0.3 kg/m^3
Gas viscosity (species A and B)	3x10^{-5} kg/m·s
Particle density	2500 kg/m^3
Particle diameter	275 µm
Grain diameter	1 µm
Bed width	0.28 m
Bed height	1 m
Static bed height	0.4 m
Fluidization velocity	0.5 m/s
Minimum fluidization velocity [19]	0.0463 m/s
Particle-particle restitution	0.9
Specularity coefficient	0.5
Initial solids packing	0.60
Maximum packing limit	0.63
Angle of internal friction	30°
Diffusion constant	1x10^{-4} m^2/s
Grid interval spacing	0.002 m (around tubes) - 0.0025 m
Time steps	1e-4 to 4e-4 s

3.6 Simulation Plan

Four sets of simulations were performed. Firstly, a grid independence study was completed in order to gauge the influence of grid spacing on the solution. The second and third simulation sets were statistical designs to investigate the effects of various independent parameters defining the setup of membranes inside the reactor. In the first of these statistical designs, the membranes were implemented only as hydrodynamic modifiers to the flow, while 50% of the fluidizing gas was injected via the membranes in the second design. The final set of simulations was a simple test of the increase in reactor performance that can be achieved by simply scaling up the reactor.

3.7 Data Collection

Reactor performance was quantified both in terms of hydrodynamics and reaction kinetics. All performance measures were time-averaged over a period of at least 15 seconds following a 10 second start-up period.

3.7.1 Pressure drop

The first hydrodynamic performance measure describes the pressure loss due to the weight of the particles being fluidized. The pressure drop was determined by averaging the time averaged static gauge pressure over the inlet since the gauge pressure at the outlet was set to zero and the pressure drop over the porous zone was negligible (~2 Pa).

3.7.2 Bed expansion ratio

This hydrodynamic performance measure gives the ratio of the averaged height of the fluidized bed to the height of the initial static bed. The average height of the fluidized bed was specified as the height at which the average value of the time-averaged solids volume fraction was 0.05.

3.7.3 Reactant exit rate

This first measure of reactor performance from a reaction kinetic point of view gives the rate at which unreacted gas species A exits the reactor. Good reactor performance will therefore be characterized by lower values of this performance measure. The mass flow rate was determined by integrating the time averaged flux of species A over the reactor outlet.

3.7.4 Equivalent reactor height

This performance measure is given as a linear representation of the reactant exit rate. Since the reaction rate in the present study is proportional to the concentration of species A, the rate will decrease as the reactant is used up along the height of the reactor. This will give an exponential relationship between the degree of conversion and the height of the reactor and will hinder accurate interpretation of results, especially at higher conversions. The statistical designs used in this paper also require linear dependent variables. It was therefore decided to express the reactor performance as the height of a reactor without any membrane insertion that would be required to achieve an equivalent degree of conversion.

In order to determine this performance measure, five different simulation runs were completed for reactors without any membrane insertion at heights of 1, 1.5, 2, 2.5 and 3 meters. The proportion of the bed taken up by the initial static bed at the bottom and the porous zone at the top was maintained for all five simulations. The mass flow rate at which species A exits the reactor was measured for each run and an exponential curve fit was made in order to establish a relation between the exponential measure of reactant conversion and the linear measure of reactor height. This curve fit is given in Figure 1.

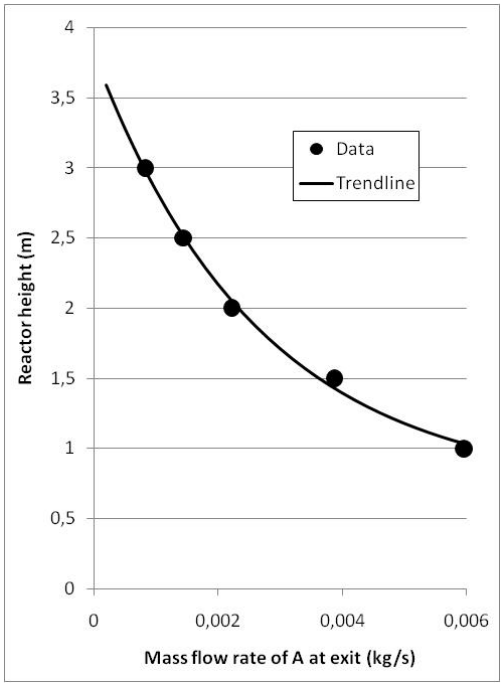

Figure 1: The relation between the mass flow rate of A at the exit and the reactor height.

The fit in Figure 1 is characterized by the relation $H_{eq} = 0.7015 + \exp\left(1.136 - 376.2\dot{m}_A\right)$. This relation can now be used to easily derive the equivalent reactor height from the reactant exit rate. This conversion results in an easily visualizable and linear measure of reactor performance.

4 Results and discussion

4.1 Grid independence study

The effect of mesh size on simulation results was investigated based on two parameters: a minimum size which was specified to finely resolve the flow around the small, circular membranes and a maximum size to which the grid can grow into the remainder of the domain. Cells were set to grow exponentially with a factor of 1.2. The reactor geometry was filled with six rows of membranes (0.01 m diameter) arranged in a staggered formation with a horizontal and vertical spacing of 0.08 m. Results of this study are given in Table 2.

The first clear observation is that grid independence is easily achieved from a hydrodynamic point of view, but not from a reaction kinetic point of view. Both hydrodynamic performance measures (pressure drop and bed expansion ratio) can be considered to be grid independent in all the cases tested. The maximum

deviations from the mean for the pressure drop and the bed expansion ratio are 1.14 and 2.08% respectively. Changes in grid spacing can therefore be concluded to have a negligible effect on the overall bed hydrodynamics.

Table 2: Results from the grid independence study. In determining the case number, the maximum size was doubled for each number from 0 to 3 and the minimum size was doubled for each letter from a to c.

Case number		3b	2c	2b	2a	1b	0a
Cell size (m)	Min	0.002	0.004	0.002	0.001	0.002	0.001
	Max	0.01	0.005	0.005	0.005	0.0025	0.00125
Number of cells		6,114	9,611	11,135	14,327	37,854	147,491
Pressure drop (Pa)		5636	5669	5660	5641	5695	5738
Bed expansion ratio		1.79	1.78	1.75	1.80	1.75	1.73
Reactant exit rate (kg/s)		0.00447	0.00477	0.00504	0.00502	0.00542	0.00576
Equivalent reactor height(m)		1.28	1.22	1.17	1.17	1.11	1.06

For the reaction kinetics, on the other hand, a clear trend of grid dependence is visible. Results indicate that the simulated reactor performance will worsen as the grid is refined. This can be seen in a gradually increasing reactant exit rate and a gradually decreasing equivalent reactor height. Such a trend is consistent with the results of Cloete *et al.* [20] where it was observed that insufficient resolution of solids structures over-predicted the gas-solid contact, thereby increasing the simulated reaction rate.

It is also clear that the effect of the minimum size is much smaller than that of the maximum size. This can be observed by comparing the results from cases 2a (1.17), 2b (1.17) and 2c (1.22) where the value in brackets indicates the equivalent reactor height in meters for the each specific case. Independence seems to be achieved already at case 2b for the minimum cell size. The maximum cell size, on the other hand, shows no sign of grid independence. By comparing cases 1b (1.11), 2b (1.17) and 3b (1.28), it can be seen that the solution is still changing substantially, even at the finest grid investigated. There are signs that grid independence is being approached, however, in that the change in solution is decreasing with a decrease in cell size. The same trend is visible when changing the minimum and maximum cell sizes simultaneously. When comparing cases 0a

(1.06), 1b (1.11) and 2c (1.22), it is clear that grid dependence is present even at the finest grid, but overall grid independence is being approached.

Unfortunately, case number 0a was already prohibitively expensive to carry out the substantial number of simulations required in this study. Therefore, case number 1b was selected as a basis for the remainder of the study. Even though significant grid dependence effects are still present on this grid, it should provide an accurate quantitative reflection of system behaviour when comparing between simulations. The same fluidization conditions and basic geometry will be used in all the studies, implying that the grid dependence effects will be similar for all cases.

4.2 Screening design without membrane gas injection

Five factors were considered in a 2^{5-2} fractional factorial design [21] and analysed in the commercial software package STATISTICA 10. In essence, a 2^{5-2} fractional factorial implies that 5 different independent variables can be evaluated using only $2^{5-2} = 2^3 = 8$ experiments. For complete information about the system, a so-called full factorial design of $2^5 = 32$ experiments will be necessary, but this particular numerical experiment will not consider any higher order interaction effects and eight simulation runs will be sufficient to estimate the primary effects. This fractional factorial design is of resolution III, implying that the primary effects may be confounded with two-factor interaction effects. Primary effects are therefore assumed to be significantly larger than interaction effects. Generally, this is a good assumption.

A factorial design examines each independent variable (generally called a factor in factorial designs) at a low and a high level and estimates the significance of making this change on some dependent variable. The 5 independent variables or factors are listed below. Factor levels were specified such that the high level should intuitively result in better reactor performance.

1. Height of membrane filling:
    a. Low: 0.24m
    b. High: 0.48m
2. Horizontal spacing between membranes:
    a. Low: 0.08m
    b. High: 0.04m
3. Vertical spacing between membranes:
    a. Low: 0.08m
    b. High: 0.04m
4. Diameter of membrane tubes:
    a. Low: 0.01m
    b. High: 0.02m
5. Arrangement of membrane tubes:

a. Low: aligned
b. High: staggered

Results from this design are summarized in Table 3.

Table 3: Model setup and simulation results for the screening design without membrane gas injection.

	Case 1	Case 2	Case 3	Case 4	Case 5	Case 6	Case 7	Case 8	
Contours of mean mass fraction of A	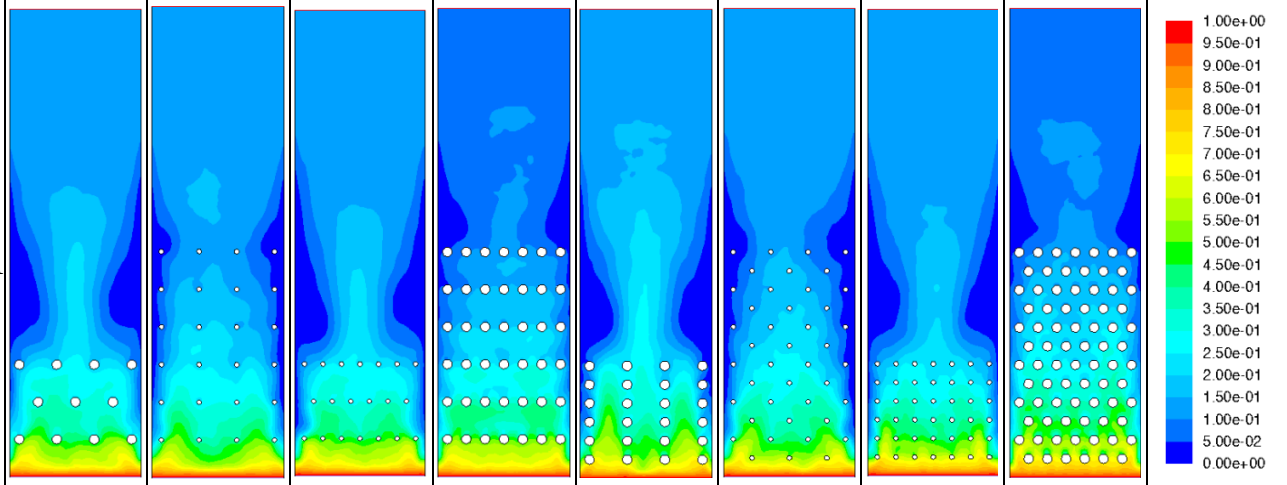								
Factor specifications	LLLHH	HLLLL	LHLLH	HHLHL	LLHHL	HLHLH	LHHLL	HHHHH	L – low H – high
Pressure drop	5606.8	5596.7	5654.1	5568.3	5432.1	5624.9	5608.2	5446.0	Pa
Expansion ratio	1.775	1.75	1.775	1.875	1.75	1.75	1.775	1.825	-
Reactant exit rate	0.005206	0.005438	0.004870	0.003714	0.005868	0.004828	0.004894	0.003743	kg/s
Equivalent height	1.14	1.10	1.20	1.47	1.04	1.21	1.20	1.46	m

The statistical design also enables the estimation of factor significance by means of an analysis of variance (ANOVA). Here, the influence of each factor can be quantified by the sum of squares. The sum of squares is an indication of the variance (i.e. the squared distance between experimental observations and the mean) within the design. By dividing the sum of squares created by a change in one factor by the total sum of squares in the design, the percentage of variance explained by each factor can be calculated.

Additionally, the significance of each factor can be quantified as a p-value. The p-value is calculated from the F-test which weighs the amount of explained variance (variance resulting from changing the factor value from low to high) against the amount of unexplained variance (variance resulting from human errors, round-off errors, averaging errors or possible interaction effects). The amount of unexplained variance is an indication of the amount of uncertainty in the design.

A large amount of uncertainty reduces the confidence with which a specific factor can be classified as significant. Thus, if the ratio of explained to unexplained variance becomes small due to a large amount of unexplained variance, the significance of the factor reduces. This significance is measured by the p-value. Typically, a p-value of 0.05 or lower is regarded as significant. A p-value of 0.05 can be interpreted as follows: if this design was repeated 100 times with the same degree of error, the opposite of the currently predicted effect would occur 5 times. Thus, the predicted effect would occur 95 out of a 100 times.

In order to get a quantitative measure of the influence of a particular factor on a dependent variable, the mean effect of changing this factor can also be calculated. This value is simply calculated as the difference between the mean resulting from the simulations at the high factor level and the mean of those at the low factor level.

Table 4: Percentage of variance, factor significance and mean effect for the equivalent reactor height performance measure in the screening design without membrane gas injection.

Factor	Percentage of variance	p-value	Mean effect (m)
1	32.0	0.044	0.167
2	50.0	0.029	0.208
3	0.0	0.972	-0.001
4	12.2	0.105	0.103
5	2.8	0.308	0.049
Error	3.0		

Table 4 shows that factors 1 (membrane height) and 2 (horizontal spacing) were found to be significant in this design. Factor 3 (vertical spacing) was found to be completely insignificant while the remaining two factors had a moderate effect. All significant factors had the expected positive impact on the equivalent reactor height when the factor level was changed from low to high.

The primary performance measure of any reactor is the degree of conversion it will achieve. The equivalent reactor height measure used in this study offers a direct quantification of the impact of membrane insertion on this performance measure. As an example, case 4 in Table 3 returned an equivalent reactor height of 1.47 m. This implies that the insertion of membranes in the way specified for case 4 into a 1 m reactor would result in the amount of conversion that can be attained in a 1.47 m reactor without any membranes. The reactor can therefore be made 47 cm shorter if the membranes are inserted.

As seen in Table 3, the membrane arrangements in cases 4 and 8 returned the best performance. The good performance of these reactors is due to high values of the three most influential factors in the design (horizontal spacing, membrane height and membrane diameter). The two most significant of these (horizontal spacing and membrane height) will now be discussed in greater detail with the aid of Figure 2. Sections a and b of Figure 2 has both these factors at their low levels (case 5) while sections c and d has these factors set to their high levels (case 4). The effect of this combined alteration is clearly quantified by a 0.43 m difference in equivalent reactor height.

The streamline plots in Figure 2 a and c clearly show the influence of the horizontal membrane spacing. It is shown that strong channelling is allowed when the horizontal spacing is large (Figure 2 a). When the spacing is reduced, however, the gas seems to rise across the entire width of the vessel. A decrease in the horizontal membrane spacing therefore has the important dual effect of reducing gas backmixing by preventing rapid central channelling and accompanying downflows at the walls, and increasing gas-solid contact by making the reacting gas rise more uniformly.

An increase in the membrane height simply increases the area of the reactor influenced by these advantages. Figure 2 b and d shows that regions without membranes quickly experience significant radial volume fraction segregation. This is the driving force for the typical recirculating flow patterns and serves to increase gas back-mixing and reduce gas solid contact.

It would theoretically be possible to improve the performance of the reactor even further, but as seen from Table 3 there is limited scope for further increasing the horizontal spacing and membrane height beyond the high levels investigated in this design. In case 8, for example, there is not much space for more membranes in the reactor. A specialized optimization study on the most significant factors identified here is recommended for future study though.

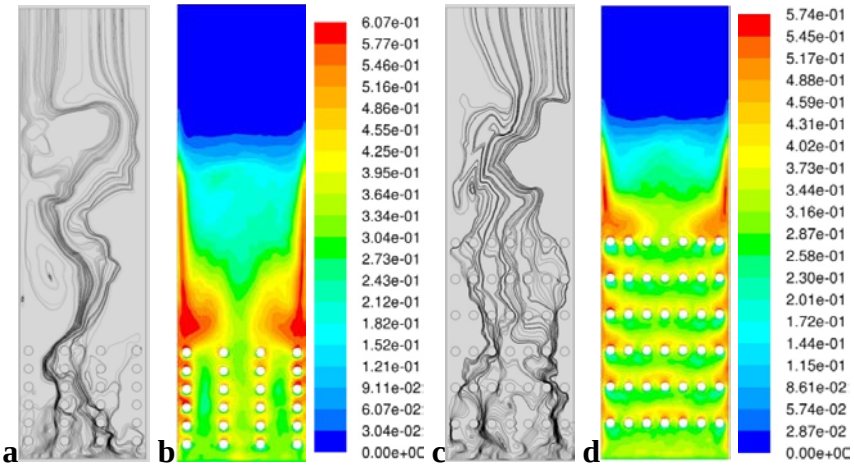

Figure 2: (a) Path lines for case 5; (b) Contours of mean volume fraction of the granular phase for case 5; (c) Path lines for case 4 (d) Contours of mean volume fraction of the granular phase for case 4

4.3 Screening design with membrane gas injection

This set of simulations was identical to that reported in the previous section, except for the way in which the gas injection was specified. In these simulations, 50 % of the fluidization gas was inserted via the membranes and the remainder via the normal inlet. Table 5 shows the ANOVA results for this design.

Table 5: Percentage of variance, factor significance and mean effect for the equivalent reactor height performance measure in the screening design with membrane gas injection.

Factor	Percentage of variance	p-value	Mean effect (m)
1	76.9	0.014	-0.141
2	11.4	0.086	0.054
3	3.9	0.205	0.032
4	0.0	0.910	0.002
5	5.6	0.156	-0.038
Error	2.2		

A comparison of Table 5 to Table 4 clearly indicates that the inclusion of gas injection through the membranes has a large, but decidedly non-linear effect on reactor performance. This is best observed from the means varying greatly in magnitude and quite often in sign between the two sets of simulations. Aside from the large effect induced by membrane injection, however, effects from the five

factors investigated are generally much lower than those observed in the screening design without gas injection. This is an indication that injection of gas through the membranes significantly reduces the possible impact that membrane arrangement can have on reactor performance.

An understanding of this observation can be gained by further analyzing the implications of membrane injection. The primary beneficial effect that can result from this alteration is that the reacting gas is injected in a much more diffuse manner throughout the reactor. This will greatly improve gas-solid contact and lead to increased reaction rates. It can therefore be envisioned that this effect can be achieved by simply making sure that membranes are present at regular intervals throughout the reactor. The exact arrangement of these membranes (represented by the five factors in the design) would be of lesser importance, as long as they are reasonably evenly spaced.

It is interesting to observe though that the only significant effect in Table 5 (factor 1 –membrane height) has a negative influence on the reactor performance. This can be explained by considering that gas injected through the membranes experience a shorter bed height and therefore has a lower residence time in the bed. The gas injection through horizontal membranes therefore implies a tradeoff between the positive effect of improved gas-solid contact and the negative effect of reduced gas residence time. From Table 5 it is clear that the negative effect is dominant when the membrane height is increased from low to high.

By comparing Table 6 to Table 3 it can be observed that, even though reactor performance is improved by gas injection through the membranes, the best performance achieved in the design (equivalent reactor height of 1.36 m for case 7) is substantially poorer than the best performance without any membrane gas injection (equivalent reactor height of 1.47 m for case 4). This is due to the negative effect of membrane height, meaning that case 7 in Table 6 did not have the beneficial dispersive influence of additional obstructions to the flow in the upper reactor regions.

In an attempt to improve this scenario, a combination of the beneficial conditions in case 4 from in the design without gas injection (Table 3) and case 7 from the design with gas injection (Table 6) was investigated by rerunning case 4 with gas injection only through the lower half of the membranes. An equivalent reactor height of 1.51 m resulted from this setup. This is slightly superior to the performance of case 4 without any membrane injection, but not sufficient to merit further investigation.

The significant reduction in gas back mixing caused by gas injection via membranes observed experimentally [10] therefore does not translate into significantly better reactor performance. As discussed previously, the reduction in gas residence time resulting from membrane gas injection cancels out these advantages in reactive systems.

Table 6: Model setup and simulation results for the screening design with membrane gas injection.

	Case 1	Case 2	Case 3	Case 4	Case 5	Case 6	Case 7	Case 8	
Contours of mean mass fraction of A	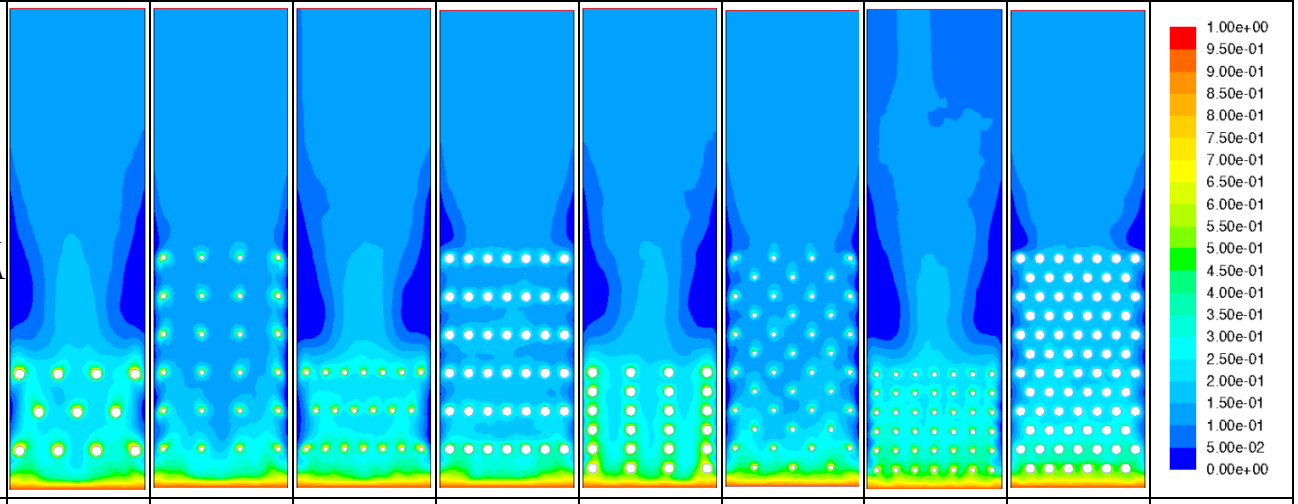								
Factor specifications	LLLHH	HLLLL	LHLLH	HHLHL	LLHHL	HLHLH	LHHLL	HHHHH	L – low H – high
Pressure drop	5657.1	5718.0	5690.2	5648.7	5594.2	5728.6	5664.4	5553.2	Pa
Expansion ratio	1.7	1.625	1.675	1.675	1.7	1.65	1.7	1.7	-
Reactant exit rate	0.004649	0.005365	0.004545	0.004940	0.004464	0.005307	0.004112	0.005062	kg/s
Equivalent height	1.24	1.12	1.26	1.19	1.28	1.12	1.36	1.17	m

4.4 Reactor scale-up

Finally, the improvements offered by a simple reactor scale-up will be investigated. Here, the reactor width will simply be increased and the injection velocity decreased proportionally in order to keep the mass flow rate of gas into the reactor constant. Results are given in Figure 3.

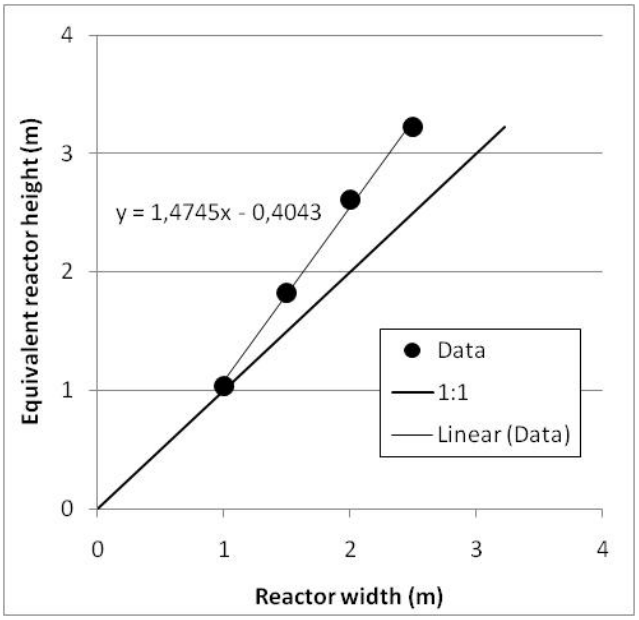

Figure 3: Effect of increased reactor width on reactor performance.

Figure 3 indicates that reactor scaling by width is significantly superior to scaling by height. Both forms of scaling increase reactor performance by increasing the gas residence time. For a height increase, the gas has a longer path to travel in the reactor while a width increase will decrease the velocity at which the gas rises through the bed. The superior performance of the reactor scaling by width, however, lies in the more dispersed way in which the gas is injected. The initial contact area over which the highly concentrated feed gas meets the bed material is enlarged by width scaling, but not by height scaling. Bubble size also becomes smaller with a decrease in fluidization velocity leading to improved gas-solid contact.

5 Conclusions

Reactive gas-solid flows within a fluidized bed with horizontally inserted membranes were simulated in order to quantify the advantages offered by the presence of membranes inside the reactor. A grid independence study was

completed before simulations were commenced to find that hydrodynamic grid independence could easily be achieved, but not reaction kinetic grid independence. This emphasized the importance of accurately resolving bubble structures in reactive fluidized bed simulations.

Simulations were carried out with a variety of membrane setups within the framework of a fractional factorial design. When the membranes served only as hydrodynamic modifiers to the flow, significant improvements to reactor performance could be obtained by changing the arrangement of membranes. A decrease in the horizontal spacing and an increase in the overall height of the membrane bundle were identified to offer the greatest improvements. The best membrane arrangement in the 1 m reactor investigated in the design achieved the same degree of conversion that would be obtained in a 1.47 m reactor without any membranes.

Even though this effect is highly significant, the use of horizontal membranes solely as hydrodynamic modifiers with which to optimise the flow patterns inside the reactor cannot be merited. The complexity and cost of inserting the horizontal hydrodynamic modifiers would far outweigh that associated with simply increasing the reactor height by 50%. For processes where the membranes play an integral part by extracting certain gas species, however, investigations into membrane arrangement are highly recommended and can lead to significant increases in reactor efficiency.

Another set of simulations were carried out where 50% of the gas was injected through the membranes. This arrangement would inject the gas in a much more dispersed manner, thereby increasing the gas-solid contact and improving reactor performance. It was found, however, that the reduction in gas residence time caused by injecting the gas closer to the surface of the bed placed some strict restrictions on the advantages offered by this approach. The performance of a 1.51 m reactor without any membranes could be matched in a 1 m reactor with injection through the membranes. Again, even though this increase in performance is significant, the costs and process complexity demanded by such an arrangement would far outweigh those from simply increasing the reactor height.

Finally, the effect of reactor scaling by width as opposed to height was investigated. It was found that scaling by width improved reactor performance significantly more than an equivalent scaling by height.

It can therefore be concluded that improvement in reactor performance can most easily and simply be obtained by increasing the reactor width. Scaling by reactor height would be the next best solution. Even though improvements gained by inserting membranes and injecting some of the reacting gas through the membranes are significant, the magnitude of these improvements is insufficient to justify the process complexity and costs associated.

6 List of Symbols

Main Symbol definitions:

α	Volume fraction
ϕ	Energy transfer rate (kg/m.s^3)
φ	Angle of internal friction
γ	Dissipation rate (kg/m.s^3)
λ	Bulk viscosity (kg/m.s)
μ	Viscosity (kg/m.s)
Θ_s	Granular temperature (m^2/s^2)
ρ	Density (kg/m^2)
ς	Specularity coefficient
$\overline{\overline{\tau}}$	Stress tensor
τ_s	Particle relaxation time (s)
$\vec{\tau}_s$	Particle shear force at the wall (N)
$\vec{\upsilon}$	Velocity vector (m/s)
υ_r	Terminal velocity (m/s)
C	Molar concentration (mol/m^3)
C_D	Drag coefficient
d	Diameter (m)
e	Restitution coefficient
f	Drag function
$\vec{g}$	Gravity vector (m/s^2)
$g_{0,ss}$	Radial distribution function
H	Reactor height (m)
$\overline{\overline{I}}$	Identity tensor
I_{2D}	Second invariant of deviatoric stress tensor
$\vec{J}$	Diffusive flux
K	Momentum exchange coefficient
k	Diffusion coefficient (kg/m·s)
k	Reaction rate constant (m/s)
M	Molar mass (kg/mol)
$\dot{m}$	Mass flow rate (kg/s)
N	Moles (mol)
p	Pressure (Pa)
R	Gas constant (J/K.mol)
R^H	Heterogeneous reaction rate (mol/m^{3}s)

Re_s	Particle slip Reynolds number
S	Source term (kg/m^{3}s)
t	Time (s)
$\vec{U}_{s,\|\|}$	Particle velocity parallel to wall (m/s)
V	Volume (m^3)
x	Mass fraction
Y	Species mass fraction

Sub- and superscript definitions:

Θ_s	Granular temperature
A	Species A
B	Species B
c	Core
eq	Equivalent
g	Gas
gr	Grain
gs	Inter-phase
i	Species index
max	Maximum packing
n	Reaction order
s	Solid
ss	Solid-solid
T	Transpose

7 References

1. Deshmukh, S.A.R.K., et al., *Membrane assisted fluidized bed reactors: Potentials and hurdles.* Chemical Engineering Science, 2007. **62**(1-2): p. 416-436.
2. Lun, C.K.K., et al., *Kinetic Theories for Granular Flow: Inelastic Particles in Couette Flow and Slightly Inerlastic Particles in a General Flow Field.* Journal of Fluid Mechanics, 1984. **140**: p. 223-256.
3. Syamlal, M., W. Rogers, and T.J. O'Brien, *MFIX Documentation: Volume 1, Theory Guide.* 1993, Springfield: National Technical Information Service.
4. Gidaspow, D., R. Bezburuah, and J. Ding, *Hydrodynamics of Circulating Fluidized Beds, Kinetic Theory Approach*, in *7th Engineering Foundation Conference on Fluidization* 1992. p. 75-82.

5. Taghipour, F., N. Ellis, and C. Wong, *Experimental and computational study of gas-solid fluidized bed hydrodynamics.* Chemical Engineering Science, 2005. **60**(24): p. 6857-6867.
6. Asegehegn, T.W. and H.J. Krautz. *Hydrodynamic Simulation of Gas-Solid Bubbling Fluidized Bed Containing Horizontal Tubes*. in *20th International Conference on Fluidized Bed Combustion*. 2010: Springer Berlin Heidelberg.
7. Jung, J. and I.K. Gamwo, *Multiphase CFD-based models for chemical looping combustion process: Fuel reactor modeling.* Powder Technology, 2008. **183**(3): p. 401-409.
8. Deng, Z., et al., *Numerical simulation of chemical looping combustion process with CaSO4 oxygen carrier.* International Journal of Greenhouse Gas Control, 2009. **3**(4): p. 368-375.
9. Yu, L., et al., *Numerical simulation of the bubbling fluidized bed coal gasification by the kinetic theory of granular flow (KTGF).* Fuel. **86**(5-6): p. 722-734.
10. Deshmukh, S.A.R.K., M. van Sint Annaland, and J.A.M. Kuipers, *Gas back-mixing studies in membrane assisted bubbling fluidized beds.* Chemical Engineering Science, 2007. **62**(15): p. 4095-4111.
11. Hull, A.S., et al., *Influence of horizontal tube banks on the behavior of bubbling fluidized beds: 1. Bubble hydrodynamics.* Powder Technology, 1999. **103**(3): p. 230-242.
12. Lun, C.K.K., et al., *Kinetic Theories for Granular Flow: Inelastic Particles in Couette Flow and Slightly Inelastic Particles in a General Flow Field.* Journal of Fluid Mechanics, 1984. **140**: p. 223-256.
13. Schaeffer, D.G., *Instability in the Evolution Equations Describing Incompressible Granular Flow*. Journal of Differential Equations, 1987. **66**: p. 19-50.
14. Ogawa, S.U., A.; Oshima, N., *On the Equation of Fully Fluidized Granular Materials.* Journal of Applied Mathematics and Physics, 1980. **31**: p. 483.
15. Levenspiel, O., *Chemical Reaction Engineering*. 3 ed. 1999: John Wiley & Sons.
16. Johnson, P.C. and R. Jackson, *Frictional-Collisional Contitutive Relations for Granular Materials, with Application to Plane Shearing.* Journal of Fluid Mechanics, 1987. **176**: p. 67-93.
17. Patankar, S., *Numerical Heat Transfer and Fluid Flow*. 1980: Hemisphere Publishing Corporation.
18. Leonard, B.P. and S. Mokhtari. *ULTRA-SHARP Nonoscillatory Convection Schemes for High-Speed Steady Multidimensional Flow*. in *NASA TM 1-2568 (ICOMP-90-12)*. 1990. NASA Lewis Research Center.

19. Bi, H.T. and J.R. Grace, *Flow regime diagrams for gas-solid fluidization and upward transport.* International Journal of Multiphase Flow, 1995. **21**(6): p. 1229-1236.
20. Cloete, S., S. Amini, and S.T. Johansen, *On the effect of cluster resolution in riser flows on momentum and reaction kinetic interaction.* Powder Technology, 2011. **210**(1): p. 6-17.
21. Montgomery, D., *Design and Analysis of Experiments*. 5 ed. 2001, New York: John Wiley and Sons.